Biomedical Optics EXPRESS

Dynamic OCT measurement of corneal deformation by an air puff in normal and cross-linked corneas

Carlos Dorronsoro,* Daniel Pascual, Pablo Pérez-Merino, Sabine Kling, and Susana Marcos

Instituto de Optica, Consejo Superior de Investigaciones Científicas (CSIC), Serrano 121, 28006 Madrid, Spain
**cdorronsoro@io.cfmac.csic.es*
www.vision.csic.es

Abstract: A new technique is presented for the non-invasive imaging of the dynamic response of the cornea to an air puff inducing a deformation. A spectral OCT instrument combined with an air tonometer in a non-collinear configuration was used to image the corneal deformation over full corneal cross-sections, as well as to obtain high speed measurements of the temporal evolution of the corneal apex. The entire deformation process can be dynamically visualized. A quantitative analysis allows direct extraction of several deformation parameters, such as amplitude, diameter and volume of the maximum deformation, as well as duration and speed of the increasing deformation period and the recovery period. The potential of the technique is demonstrated on porcine corneas in vitro under constant IOP for several conditions (untreated, after riboflavin instillation and under cross-linking with ultraviolet light), as well as on human corneas in vivo. The new technique has proved very sensitive to detect differences in the deformation parameters across conditions. We have confirmed non-invasively that Riboflavin and UV-cross-linking induce changes in the corneal biomechanical properties. Those differences appear to be the result of changes in constituent properties of the cornea, and not a consequence of changes in corneal thickness, geometry or IOP. These measurements are a first step for the estimation of the biomechanical properties of corneal tissue, at an individual level and in vivo, to improve diagnosis and prognosis of diseases and treatments involving changes in the biomechanical properties of the cornea.

OCIS codes: (330.5370) Physiological optics; (330.4460) Ophthalmic optics and devices; (170.4470) Ophthalmology; (170.4500) Optical coherence tomography; (170.3880) Medical and biological imaging.

References and links

1. T. T. Andreassen, A. Hjorth Simonsen, and H. Oxlund, "Biomechanical properties of keratoconus and normal corneas," Exp. Eye Res. **31**(4), 435–441 (1980).
2. W. J. Dupps, Jr. and S. E. Wilson, "Biomechanics and wound healing in the cornea," Exp. Eye Res. **83**(4), 709–720 (2006).
3. Y. S. Rabinowitz, "Keratoconus," Surv. Ophthalmol. **42**(4), 297–319 (1998).
4. E. Spoerl, M. Huhle, and T. Seiler, "Induction of cross-links in corneal tissue," Exp. Eye Res. **66**(1), 97–103 (1998).
5. G. Wollensak, E. Spoerl, and T. Seiler, "Riboflavin/ultraviolet-a-induced collagen crosslinking for the treatment of keratoconus," Am. J. Ophthalmol. **135**(5), 620–627 (2003).
6. G. Wollensak, E. Spoerl, and T. Seiler, "Stress-strain measurements of human and porcine corneas after riboflavin-ultraviolet-A-induced cross-linking," J. Cataract Refract. Surg. **29**(9), 1780–1785 (2003).
7. J. Colin, B. Cochener, G. Savary, and F. Malet, "Correcting keratoconus with intracorneal rings," J. Cataract Refract. Surg. **26**(8), 1117–1122 (2000).

#159961 - $15.00 USD Received 13 Dec 2011; revised 17 Jan 2012; accepted 17 Jan 2012; published 9 Feb 2012

8. J. J. Nichols, M. M. Marsich, M. Nguyen, J. T. Barr, and M. A. Bullimore, "Overnight orthokeratology," Optom. Vis. Sci. **77**(5), 252–259 (2000).
9. D. M. Choi, R. W. Thompson, Jr., and F. W. Price, Jr., "Incisional refractive surgery," Curr. Opin. Ophthalmol. **13**(4), 237–241 (2002).
10. C. Roberts, "The cornea is not a piece of plastic," J. Refract. Surg. **16**(4), 407–413 (2000).
11. P. S. Binder, "Ectasia after laser *in situ* keratomileusis," J. Cataract Refract. Surg. **29**(12), 2419–2429 (2003).
12. C. Deenadayalu, B. Mobasher, S. D. Rajan, and G. W. Hall, "Refractive change induced by the LASIK flap in a biomechanical finite element model," J. Refract. Surg. **22**(3), 286–292 (2006).
13. M. P. Holzer, A. Mannsfeld, A. Ehmer, and G. U. Auffarth, "Early outcomes of INTRACOR femtosecond laser treatment for presbyopia," J. Refract. Surg. **25**(10), 855–861 (2009).
14. B. Jue and D. M. Maurice, "The mechanical properties of the rabbit and human cornea," J. Biomech. **19**(10), 847–853 (1986).
15. D. A. Hoeltzel, P. Altman, K. Buzard, and K. Choe, "Strip extensiometry for comparison of the mechanical response of bovine, rabbit, and human corneas," J. Biomech. Eng. **114**(2), 202–215 (1992).
16. A. Elsheikh and K. Anderson, "Comparative study of corneal strip and extensiometry and inflation tests," J. R. Soc. Interface **46**(2), 409–414 (2005).
17. A. Elsheikh, D. Alhasso, and P. Rama, "Biomechanical properties of human and porcine corneas," Exp. Eye Res. **86**(5), 783–790 (2008).
18. K. Anderson, A. El-Sheikh, and T. Newson, "Application of structural analysis to the mechanical behaviour of the cornea," J. R. Soc. Interface **1**(1), 3–15 (2004).
19. H. Hennighausen, S. T. Feldman, J. F. Bille, and A. D. McCulloch, "Anterior-posterior strain variation in normally hydrated and swollen rabbit cornea," Invest. Ophthalmol. Vis. Sci. **39**(2), 253–262 (1998).
20. W. Śródka and D. R. Iskander, "Optically inspired biomechanical model of the human eyeball," J. Biomed. Opt. **13**(4), 044034 (2008).
21. S. Kling, L. Remon, A. Pérez-Escudero, J. Merayo-Lloves, and S. Marcos, "Corneal biomechanical changes after collagen cross-linking from porcine eye inflation experiments," Invest. Ophthalmol. Vis. Sci. **51**(8), 3961–3968 (2010).
22. A. Elsheikh and D. Alhasso, "Mechanical anisotropy of porcine cornea and correlation with stromal microstructure," Exp. Eye Res. **88**(6), 1084–1091 (2009).
23. S. Kling, J. J. del Coz, P. Pérez-Merino, J. L. Suarez, and S. Marcos, "Impact of hydration state and storage media on corneal biomechanical properties from in vitro inflation tests and finite element modeling," submitted to Invest. Ophthalmol. Vis. Sci.
24. D. A. Luce, "Determining in vivo biomechanical properties of the cornea with an ocular response analyzer," J. Cataract Refract. Surg. **31**(1), 156–162 (2005).
25. B. M. Fontes, R. Ambrósio, Jr., G. C. Velarde, and W. Nosé, "Ocular response analyzer measurements in keratoconus with normal central corneal thickness compared with matched normal control eyes," J. Refract. Surg. **27**(3), 209–215 (2011).
26. Y. Goldich, Y. Barkana, Y. Morad, M. Hartstein, I. Avni, and D. Zadok, "Can we measure corneal biomechanical changes after collagen cross-linking in eyes with keratoconus?--a pilot study," Cornea **28**(5), 498–502 (2009).
27. G. Grabner, R. Eilmsteiner, C. Steindl, J. Ruckhofer, R. Mattioli, and W. Husinsky, "Dynamic corneal imaging," J. Cataract Refract. Surg. **31**(1), 163–174 (2005).
28. M. R. Ford, W. J. Dupps, Jr., A. M. Rollins, A. S. Roy, and Z. Hu, "Method for optical coherence elastography of the cornea," J. Biomed. Opt. **16**(1), 016005–016007 (2011).
29. X. He and J. Liu, "A quantitative ultrasonic spectroscopy method for noninvasive determination of corneal biomechanical properties," Invest. Ophthalmol. Vis. Sci. **50**(11), 5148–5154 (2009).
30. R. Ambrósio, Jr., L. P. Nogueira, D. L. Caldas, B. M. Fontes, A. Luz, J. O. Cazal, M. R. Alves, and M. W. Belin, "Evaluation of corneal shape and biomechanics before LASIK," Int. Ophthalmol. Clin. **51**(2), 11–38 (2011).
31. C. J. Roberts, A. M. Mahmoud, I. Ramos, D. Caldas, R. Siqueira da Silva, and R. Ambrósio, Jr., "Factors influencing corneal deformation and estimation of intraocular pressure," in ARVO (2011), pp. E-abstract 4384.
32. M. Dubbelman, H. A. Weeber, R. G. van der Heijde, and H. J. Völker-Dieben, "Radius and asphericity of the posterior corneal surface determined by corrected Scheimpflug photography," Acta Ophthalmol. Scand. **80**(4), 379–383 (2002).
33. P. Rosales and S. Marcos, "Pentacam Scheimpflug quantitative imaging of the crystalline lens and intraocular lens," J. Refract. Surg. **25**(5), 421–428 (2009).
34. A. Pérez-Escudero, C. Dorronsoro, L. Sawides, L. Remón, J. Merayo-Lloves, and S. Marcos, "Minor influence of myopic laser in situ keratomileusis on the posterior corneal surface," Invest. Ophthalmol. Vis. Sci. **50**(9), 4146–4154 (2009).
35. J. A. Izatt, M. R. Hee, E. A. Swanson, C. P. Lin, D. Huang, J. S. Schuman, C. A. Puliafito, and J. G. Fujimoto, "Micrometer-scale resolution imaging of the anterior eye in vivo with optical coherence tomography," Arch. Ophthalmol. **112**(12), 1584–1589 (1994).
36. R. F. Steinert and D Huang, eds., *Anterior Segment Optical Coherence Tomography* (SLACK Incorporated, Thorofare, N.J., 2008).

#159961 - $15.00 USD Received 13 Dec 2011; revised 17 Jan 2012; accepted 17 Jan 2012; published 9 Feb 2012

37. M. Gora, K. Karnowski, M. Szkulmowski, B. J. Kaluzny, R. Huber, A. Kowalczyk, and M. Wojtkowski, "Ultra high-speed swept source OCT imaging of the anterior segment of human eye at 200 kHz with adjustable imaging range," Opt. Express **17**(17), 14880–14894 (2009).
38. I. Grulkowski, M. Gora, M. Szkulmowski, I. Gorczynska, D. Szlag, S. Marcos, A. Kowalczyk, and M. Wojtkowski, "Anterior segment imaging with Spectral OCT system using a high-speed CMOS camera," Opt. Express **17**(6), 4842–4858 (2009).
39. D. Alonso-Caneiro, K. Karnowski, B. J. Kaluzny, A. Kowalczyk, and M. Wojtkowski, "Assessment of corneal dynamics with high-speed swept source optical coherence tomography combined with an air puff system," Opt. Express **19**(15), 14188–14199 (2011).
40. S. Ortiz, D. Siedlecki, I. Grulkowski, L. Remon, D. Pascual, M. Wojtkowski, and S. Marcos, "Optical distortion correction in optical coherence tomography for quantitative ocular anterior segment by three-dimensional imaging," Opt. Express **18**(3), 2782–2796 (2010).
41. J. M. Bueno, E. J. Gualda, A. Giakoumaki, P. Pérez-Merino, S. Marcos, and P. Artal, "Multiphoton microscopy of ex vivo corneas after collagen cross-linking," Invest. Ophthalmol. Vis. Sci. **52**(8), 5325–5331 (2011).
42. I. G. Pallikaris, G. D. Kymionis, H. S. Ginis, G. A. Kounis, and M. K. Tsilimbaris, "Ocular rigidity in living human eyes," Invest. Ophthalmol. Vis. Sci. **46**(2), 409–414 (2005).
43. M. Doors, N. G. Tahzib, F. A. Eggink, T. T. J. M. Berendschot, C. A. B. Webers, and R. M. M. A. Nuijts, "Use of anterior segment optical coherence tomography to study corneal changes after collagen cross-linking," Am. J. Ophthalmol. **148**(6), 844–851.e2 (2009).

1. Introduction

The mechanical properties of the cornea and its constituent materials are essential to relate its geometrical (and therefore optical) properties with its mechanical behavior [1,2]. Several corneal diseases, such as keratoconus [3], which lead to corneal deformation and thinning, affect dramatically the mechanical behavior of the cornea, and several treatments for these diseases attempt at modulating its biomechanical response. For example, an emerging treatment for keratoconus is the UV-Riboflavin cross-linking procedure, which aims at stiffening the weakened keratoconic corneas by creating intra and extrafibrillar bonds in the stromal collagen [4–6]. Other treatments such as implantation of intra-stromal rings aim at creating a supporting structure of the cornea, producing a flattening and a symmetrization of the anterior corneal surface [7]. This treatment may be highly dependent on the biomechanical properties of the cornea.

Other corneal treatments largely rely on the biomechanical corneal response to produce (more or less permanent) refractive or corneal shape changes. For example, overnight orthokeratology uses reversed geometry contact lenses to reshape the cornea to correct low amounts of refractive errors [8]. Incisional refractive surgery [9], now of limited use because of its low predictability, relied completely on the biomechanical properties of the cornea. Corneal biomechanics is claimed to play a role (in combination with the ablation algorithm and laser-corneal tissue interactions) in the achieved corneal shape following laser refractive surgery, and particularly the corneal ectasia (corneal protrusion) developed post-LASIK by some patients [10–12]. Emergent corneal procedures for presbyopia (i.e. femtosecond Intracor treatment [13,14]) aiming at producing a change in corneal curvature in the central cornea, while maintaining its integrity, rely entirely on the biomechanical properties of the treated corneas.

Despite the great need for the understanding and availability of corneal biomechanical parameters at the individual level, most of the data available today come from in vitro measurements of corneal biomechanics [14–21]. In vitro measurements have proved to be largely dependent on the technique used (with orders of magnitude differences in the reported corneal Young modulus of elasticity) and the experimental conditions (time post-mortem, hydration conditions, storage solutions, etc.). Although large efforts have been directed to the development of new paradigms for the analysis of experimental inflation data, in combination with more sophisticated models (corneal finite element models or corneal Micro-structure constituent based models [16,21–23]) the practical use of corneal biomechanical models have been somewhat limited by the reliability of the experimental input data and their validation.

With no doubt, the understanding of corneal biomechanical properties, and the practical use of corneal biomechanical models will largely benefit from in vivo measurements. Many in

#159961 - $15.00 USD Received 13 Dec 2011; revised 17 Jan 2012; accepted 17 Jan 2012; published 9 Feb 2012

vitro measurements require corneal excision and suppression of natural boundaries [14–16], and all methods suffer inevitably from unnatural corneal hydration states [19,23]. Also, customized knowledge of the biomechanical properties at the individual level would allow incorporation of custom data into corneal biomechanical models and, in consequence, a better predictability of the outcomes. Knowledge of the corneal biomechanical properties at the individual level would allow, for example, a better selection of LASIK surgery candidates (identifying potential patients at risk of corneal ectasia), customization of intrastromal ring segments, deeper understanding of corneal biomechanics-modulating treatments or diagnosis and prognosis of keratoconus.

The most important attempt to date to provide a clinical instrument to monitor the biomechanical response of the cornea has been the Ocular Response Analyzer (ORA, Reichert Ophthalmic Instruments, Buffalo, New York, USA) [24]. This instrument, an evolution of an air-puff tonometer, measures the changes in the light intensity recorded on a detector that collects light reflected from the cornea during the applanation produced by an air-puff impinging the cornea. The instrument derives values of the inward and outward pressure obtained during the dynamic applanation, which as a result of the viscous damping of the cornea, produces a delayed response. This difference is referred by the manufacturer as corneal hysteresis, due to its (indirect) relationship with corneal properties. Reports in the literature raise questions on the sensitivity of the technique to monitor changes in the biomechanical properties of the cornea. For example, there is conflicting evidence that the ORA is effective in identifying keratoconic patients [24,25] or in detecting changes with cross-linking [26]. In general, the Ocular Response Analyzer does not provide a direct measure of corneal deformation upon applanation, nor a direct measurement of standard biomechanical parameters that describe the mechanical behavior of a material. Other approaches that have been suggested include Placido-ring based topography with applanation produced by a cantilever [27], optical coherence elastography [28] and ultrasonic spectroscopy [29].

Very recently, new approaches have been presented that attempt to overcome the lack of more direct measurements of corneal deformation in vivo, although the techniques are still at early stages. Oculus has recently presented a new high-speed Scheimpflug camera capable of imaging dynamic corneal deformation upon applanation with an air-puff. The instrument has not been yet widely released clinically, and the few available reports remain mainly qualitative [30,31]. Scheimpflug imaging suffers from severe geometrical distortion and by optical distortions (in the posterior corneal surface) which need to be corrected before extracting quantitative information [32–34].

An alternative to anterior segment imaging in the eye to the Scheimpflug camera is optical coherence tomography (OCT) [35,36]. OCT has larger axial (and potentially lateral) resolution than Scheimpflug imaging, and high-speed OCT allows acquisitions of more than 100.000 A-scans/s [37,38]. The combination of OCT technology with air-puff applanation has been recently published [39]. Despite the high-speed capabilities of the OCT system employed, the data obtained with their collinear configuration are limited to the dynamic acquisition of A-scans at the corneal apex, although in principle the technique could be applied on a larger corneal region (of primary interest for understanding full corneal dynamics).

In this work, we present a new development of spectral OCT (sOCT) technology combined with air-puff applanation which allows monitoring corneal deformation over full corneal cross-sections, besides high speed imaging of the corneal apex. We demonstrate the potential of the technique in vitro on porcine corneas, as well as in vivo in humans. In particular, we show the sensitivity of the technique to detect differences in corneal deformation between virgin corneas, corneas treated with Riboflavin + Dextran, and corneas after a UV-cross-linking procedure. These measurements are a first step for the estimation of corneal constituent material properties in vivo.

#159961 - $15.00 USD Received 13 Dec 2011; revised 17 Jan 2012; accepted 17 Jan 2012; published 9 Feb 2012

2. Methods

2.1. Instrument implementation

A commercial non-contact tonometer (NT 2000, Nidek, Hiroishi, Japan) was combined with a custom spectral domain OCT system (previously described by Grulkowski et al. [38]) to provide dynamic images of the corneal deformation event during an air puff. The non-contact tonometer provides an air puff which is directly impacting the cornea and produces a fast (~20 ms) deformation event, identical to that used in non-contact corneal tonometry. A tilted mirror is attached to the tube tip providing the air puff (see Fig. 1 for a schematic diagram of the setup) to allow acquisition of sOCT images.

The implementation and use of the custom-developed high-resolution sOCT instrument is described in detail elsewhere [38,40]. The axial range of the instrument is 7 mm in depth, resulting in a theoretical pixel resolution of 3.42 µm in air. The axial resolution predicted by the bandwidth of the superluminescent diode laser source (centered at 840 nm; Superlum, Ireland) is 6.9 µm. The superluminiscent diode power was set to 1.5 mW for the in vitro measurements, and to 1.0 mW for the in-vivo measurements. The acquisition time of the camera (12-bit line-scan CMOS with 4096 pixels; spL4096-140k by Basler AG, Germany) was set to 15 µs to provide high speed imaging of the cornea. Two configurations of the sOCT instrument were used to capture the dynamic behavior of the cornea: (1) 1-D measurements at full temporal resolution (every 15 µs) on the corneal apex, i.e. continuous A-scan recordings without moving the scanner; and (2) 2-D dynamic measurements (B-scans) of the horizontal meridians of the cornea. The lateral range of the B-scans was 15 mm, sampled with 90 A-scans. With this configuration, the cornea was spatially sampled every 0.17 mm, and each corneal point was temporally sampled every 1.35 ms.

The tube tip of the non-contact tonometer was placed at 11-mm from the eye, similarly to the configuration for corneal tonometry, to ensure a standard air puff on the cornea. The air puff configuration was set to a similar level in all experiments ("60 Manual" according to the denomination of the instrument used). The corneal deformation sensors of the tonometer were deactivated. In this configuration each air puff is released with the highest air pressure provided by the instrument. The tonometer measurement button was electronically controlled to provide a remote measurement trigger. The air tube tip of the instrument was rebuilt to allow the fixation of a mirror.

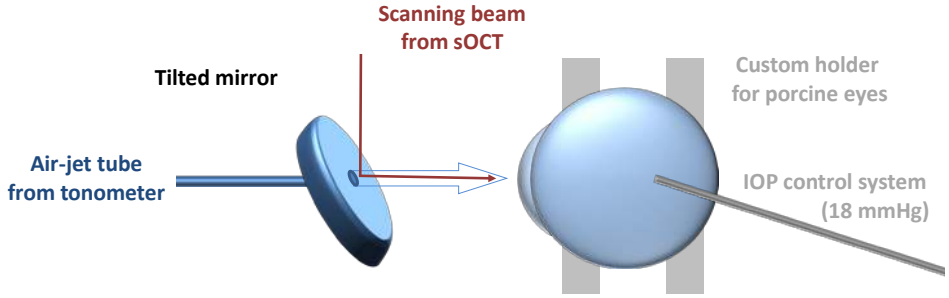

Fig. 1. Detail of the setup used in the experiments (viewed from above). A tilted mirror is fixed to the tube tip of a modified non-contact air tonometer, and provides an optical channel to a custom sOCT imaging instrument (see text for details and angles). In vivo and in vitro eyes were measured. A custom eye holder and an intraocular pressure control system (both in gray) were used in the in vitro eyes.

The mirror has a tilt angle in the horizontal direction of 45° with respect both to the tonometer and the sOCT instrument, to allow both instruments to point at the corneal apex (see Fig. 1). The mirror has an additional tilt of 8° with respect to the vertical direction, which prevents the horizontal scanning beam of the sOCT from vignetting by the hole in the mirror

#159961 - $15.00 USD Received 13 Dec 2011; revised 17 Jan 2012; accepted 17 Jan 2012; published 9 Feb 2012

that allows the air puff to reach the cornea. These mirror angles were set by the mirror drilling angle, produced at a precision mechanical workshop.

As a result of this geometrical configuration, there is a small angle (~8°) between the sOCT measurement beam axis and the air puff direction when both point at the corneal apex. In the experiments, the measurement (imaging) axis was used as a reference for the alignment of the eyes (both human in vivo and porcine in vitro). Although the resulting slightly non-normal incidence of the air puff could potentially reduce corneal deformation, this reference is preferred, since it does not induce additional distortion in the images, maintaining the symmetry of the deformation in the scanning direction (horizontal meridians). During the deformation, the air puff gets slightly decentered with respect to the corneal center defined by the imaging axis, but only 140 μm per axial millimeter of corneal displacement. This shift can be considered negligible in comparison with the much wider corneal area in which the air pulse applies a constant force.

The current configuration in which the tube tip is attached to the mirror produces slight vibrations during the air-puff release (reduced by absorbing elements disposed in the instrument holder). However, we have not observed any effect of those on the measurements during the deformation event.

2.2. IOP control system

All in vitro measurements were performed under constant IOP pressure (18 ± 1 mmHg). This was achieved by means of an automated custom pressure control system [21]. The IOP was adjusted by a pumping system (NE-500, New Era Pump Systems, Inc., Wantagh, NY), and the pressure monitored with a pressure sensor. A needle was introduced through the optical nerve head, and connected the eye to the pumping system and a water column (filled with 0.9% NaCl solution).

2.3. Calibration and validation

Three calibration and validation measurements were performed to detect potential artifacts in the images due to mirror movements or misalignments: (1) Dynamic imaging of the position of the mirror hole/tube tip during the air puff; (2) Measurement of a flat surface and rubber tonometry-probe eyes; (3) Repeated extended measurements of an in vitro eye.

The potential effect of mirror vibrations was evaluated with measurements on rigid flat surfaces. Correct alignment was adjusted and validated when the images of a flat surface appeared un-distorted, and the deformation of the probe eye symmetrical. High measurement repeatability was obtained during 3 hours (every 10 min). Increased variability after 3 hours of measurements was attributed to changes in the hydration properties of the eyes.

2.4. Eyes and measurements

Measurements were obtained on one eye of a 39-year old normal subject in vivo, and on fresh porcine enucleated eyes (virgin and after treatment) in vitro. Both in vivo and in vitro measurements were performed under similar instrumental conditions. Each measurement was repeated 5 times. The dynamic 2-D B-scan measurement mode (along the horizontal meridian) provides insights on the relative alignment of the eye with the air puff and the measuring instrument (sOCT), and therefore it was routinely used to obtain an optimal alignment before the 1-D measurements at full temporal resolution on the corneal apex.

In measurements in vivo, the subject fixated a stimulus in the sOCT instrument. The subject was stabilized using a chin-rest. The study was approved by Institutional Review Boards and followed the tenets of the Declaration of Helsinki. The subject signed a consent form and was aware of the nature of the study.

In measurements in vitro a custom eye holder allowed alignment of the eye to the instrument as well as implementing the IOP control system. The porcine eyes were obtained from a local slaughterhouse. A total of 6 eyes were used in the study. All eyes were initially

#159961 - $15.00 USD Received 13 Dec 2011; revised 17 Jan 2012; accepted 17 Jan 2012; published 9 Feb 2012

measured untreated. The corneas were then de-epithelialized. Subsequent measurements were conducted after de-epitheliazation only (1 eye), after de-epitheliazation and instillation of Riboflavin 0.125% + Dextran 20% solution during 30 minutes every 5 minutes (4 eyes), and after the full standard UV-cross-linking procedure with 3 mW/cm^2 365-nm UV-A radiation, as described in Ref. [21] (2 eyes). All in vitro measurements were performed between 2 and within 6 hours post-mortem. Between measurements the eyes were kept in a refrigerator at 4°C in a chamber with cotton soaked in physiological saline (sodium chloride 0.9%).

2.5. Data Analysis

Figure 2 represents schematic views of the type of images resulting from the measurements, and the parameters obtained for subsequent analysis. Figure 2a shows the dynamics of the apex (A-scans) throughout time. Figure 2.b depicts the corneal meridians (B-scans) before and during the deformation.

The image pixels where re-scaled in the vertical direction to provide absolute values of depth (in millimeters), and in the horizontal direction to obtain absolute values of time (Fig. 2.a; in milliseconds) and axial position (Fig. 2.b; in millimeters).

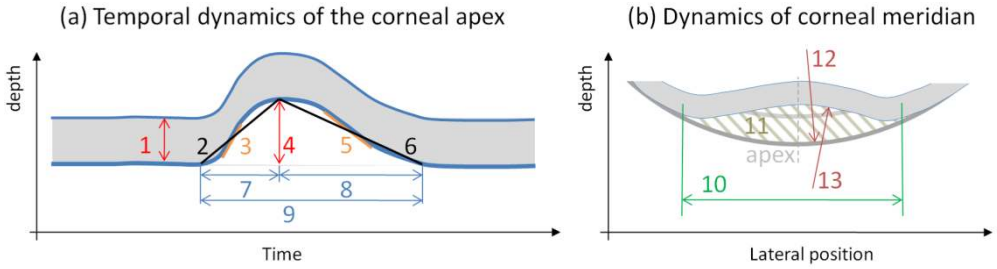

Fig. 2. Diagram of the images resulting from the measurements and the corresponding extracted parameters. (a) Measurements of the temporal dynamics of the apex (A-scans) and (b) Measurements of the dynamics (B-scans) of a corneal meridian. 1: Corneal thickness. 2: Mean deformation speed during the increasing deformation period. 3: Peak speed (maximum slope) of the increasing deformation period. 4: Deformation amplitude (peak deformation, dividing the periods of increasing and decreasing deformation). 5: Peak speed of the decreasing deformation period. 6: Mean speed of the decreasing deformation period. 7: Duration of the increasing deformation period. 8: Duration of the decreasing deformation period. 9: overall duration of the deformation event. 10: Diameter of the deformed zone. 11: Displaced volume. 12: Non-deformed corneal radius. 13: Deformed corneal radius. See text for details.

Custom routines were developed to extract quantitative parameters from the captured set of images. The analysis is based on a direct comparison between the stable non-deformed cornea immediately before the deformation event, and the corneal deformation during the air puff. The *corneal thickness* (1, red) is obtained as the axial distance between the anterior and posterior surface of the cornea, evaluated at the corneal apex before the deformation, during maximum deformation, and immediately after the deformation. The *deformation amplitude* (4, red) at the corneal apex represents the maximum deformation depth. This instant of maximum deformation (corresponding to the moment when the deformation stops increasing and starts decreasing, i.e., when the cornea starts recovering) divides the *overall deformation* (9) event in two intervals: the *increasing deformation period* (7) and the *decreasing deformation period* (8). The *mean increasing and decreasing deformation speeds* (2 and 6, black) are obtained as the deformation amplitude divided by the duration of the corresponding increasing or decreasing deformation period (slopes of the black lines in Fig. 2a). The *peak deformation speeds* (3 and 5, orange) are also obtained for the increasing and decreasing deformation periods (as the maximum positive and negative slopes of the deformation curve, represented as orange lines in Fig. 2a).

The parameters above were obtained from high-speed A-scan measurements at the corneal apex throughout (Fig. 2a). Additional information could be extracted from the dynamic B-

#159961 - $15.00 USD Received 13 Dec 2011; revised 17 Jan 2012; accepted 17 Jan 2012; published 9 Feb 2012

scan measurements (along the horizontal meridian; Fig. 2b). This imaging mode provided a direct view of the spatial deformation of the cornea. Although this corneal meridian measurement mode could potentially provide similar results about the apex dynamics than the A-scan measurements, the temporal sampling achievable is much lower and therefore the extracted parameters have lower precision. The B-scans were used to obtain the *diameter of the deformed zone* (10, green), the *displaced corneal volume* at the moment of peak deformation (11, gray), the *non-deformed corneal radius* (12) and the *peak deformed corneal radius* (13).

3. Results

3.1. Examples

Figure 3 shows three examples of dynamic A-scan measurements at the corneal apex on the same in vitro porcine eye before (Fig. 3a) and after treatments with Riboflavin (Fig. 3b) and UV-cross-linking (Fig. 3c).

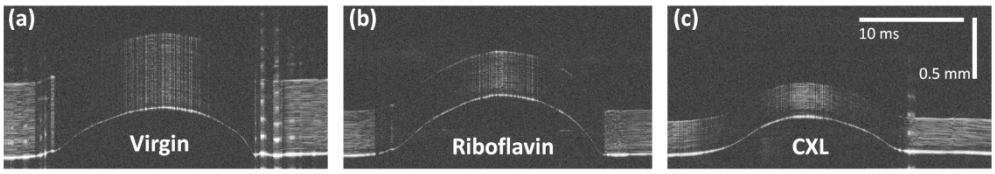

Fig. 3. Examples of dynamic A-scan measurements on the same porcine eye in vitro, (a) before and (b) after treatments of Riboflavin and (c) UV-cross-linking (c). The vertical axis represents axial depth (with the anterior corneal surface down) and the horizontal axis represents time.

Figure 4 (and Media 1) shows B-scan measurements of the same cornea. As seen in Media 1, several images are captured during the corneal deformation event. The two extreme deformation conditions shown in Fig. 4 were used to extract the quantitative deformation parameters: the image of the stable non-deformed cornea (reference condition), shown in red; and the image of the maximum transient deformed cornea, overlapped in green.

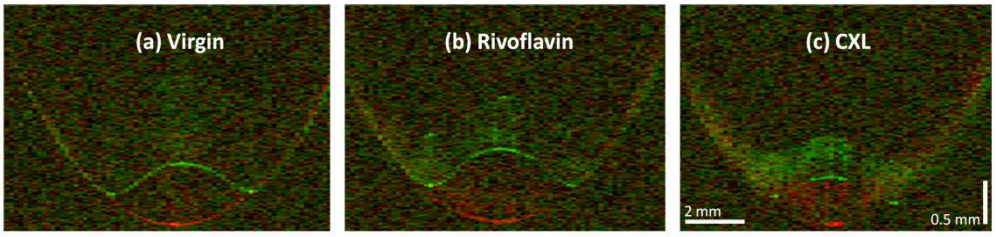

Fig. 4. Single-frame excerpts from an example video recording (Media 1) of the dynamics of horizontal sections of the cornea (B-scans), for three different conditions of the same in vitro porcine eye: (a) virgin eye with no treatment; (b) after instillation of Riboflavin; and (c) after UV-cross-linking. The stable non-deformed cornea (reference condition) is shown in red, and the deformed cornea is overlapped in green.

Figures 3 and 4 show the capability of the proposed methodology to retrieve information of the dynamic response of the cornea, with sufficient temporal (A-scans) and spatial (B-scans) resolution to extract quantitative parameters that describe the corneal deformation as a result of a 20-ms air-puff. The air-puff (conventionally used in tonometry) produces a very relevant corneal deformation in all conditions, although differences in the temporal and spatial shape of the corneal deformation occur across conditions.

3.2. Deformation amplitude and corneal thickness

Figure 5a shows the deformation amplitude and the corneal thickness for the different conditions: human eye in vivo (in green), and porcine corneas (untreated in deep blue, after

#159961 - $15.00 USD Received 13 Dec 2011; revised 17 Jan 2012; accepted 17 Jan 2012; published 9 Feb 2012

instillation of Riboflavin in neutral blue, and after UV-cross-linking in light blue). The deformation amplitude in the living human cornea was 0.56 ± 0.04 mm. Untreated porcine eyes experienced a larger deformation (0.85 ± 0.26 mm on average). The porcine corneas instilled with Riboflavin showed a mean deformation amplitude similar to that of virgin porcine eyes, although with less variability across eyes (0.87 ± 0.09 mm). After UV-cross-linking (CXL), the deformation amplitude was 0.61 ± 0.01 mm, significantly lower ($p<0.02$) than in untreated porcine eyes.

These deformation amplitudes are affected by corneal thickness. The measured human corneal thickness was 0.76 ± 0.01 mm, higher than the corresponding deformation amplitude. In porcine corneas, the instillation of Riboflavin + Dextran produced a strong reduction in corneal thickness (from 1.19 ± 0.03 mm in virgin eyes to 0.62 ± 0.05 mm), consistent with the de-hydration effects produced by Dextran [23,41]. UV-cross-linking produced further decrease in corneal thickness (down to 0.56 ± 0.02 mm).

Corneal thickness was measured before the deformation event (results described above), as well as at the moment of maximum deformation and immediately after the recovery. The difference in thickness (during and after the deformation, with respect to the thickness before the deformation, averaged across eyes in the same condition) was negative in all cases (Untreated, Riboflavin and UV-cross-linking). The thickness difference ranged between –0.007 and –0.07 mm, suggesting a slight reduction in corneal thickness during and after the applanation. However, this difference was only statistically significant (paired t-test) in two cases: human eye after the deformation (–0.074 ± 0.044 mm, $p = 0.005$); and untreated porcine cornea during the deformation (–0.023 ± 0.017, $p = 0.02$).

The ratio of deformation amplitude/corneal thickness (Fig. 5b) was similar for the untreated corneas, but changed with treatments. The deformation amplitude was lower than corneal thickness in untreated corneas, whereas it was higher for corneas instilled with Riboflavin and of the same magnitude in UV-cross-linked corneas.

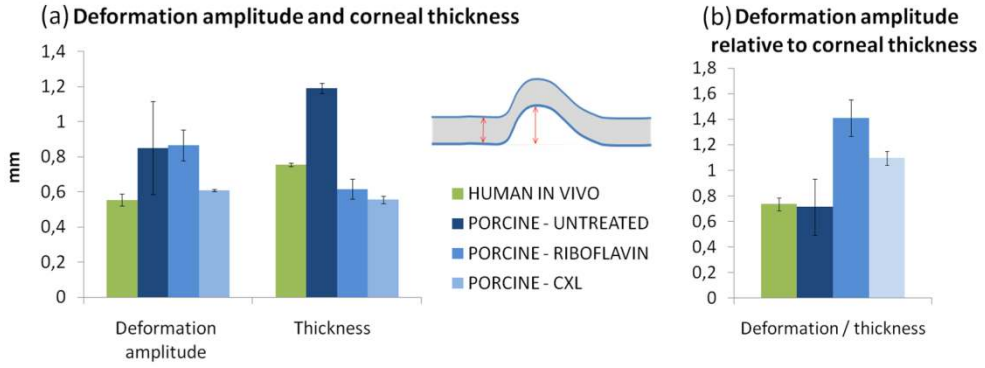

Fig. 5. (a) Deformation depth and corneal thickness (measured before the deformation event) at the corneal apex, in millimeters, for the different conditions. (b) Deformation amplitude / corneal thickness ratio. Error bars for the human eye in vivo (green columns) indicate the standard deviation across measurements for the same eye. Error Bars for porcine eyes in vitro (blue columns) indicate the standard deviations across measurements on different eyes.

3.3. Deformation time

It is interesting to note that the pulse duration (obtained from calibration measurements with the same setup) was longer (~20 ms) than the duration of the overall corneal deformation event measured: 14.3 ± 0.8 ms for the human eye in vivo and 17.3 ± 1.2 ms for the untreated porcine eyes.

The different treatments applied to the porcine eyes (Riboflavin and UV-cross-linking) did not significantly affect the overall deformation duration, as shown in Fig. 6, but changed the

#159961 - $15.00 USD Received 13 Dec 2011; revised 17 Jan 2012; accepted 17 Jan 2012; published 9 Feb 2012

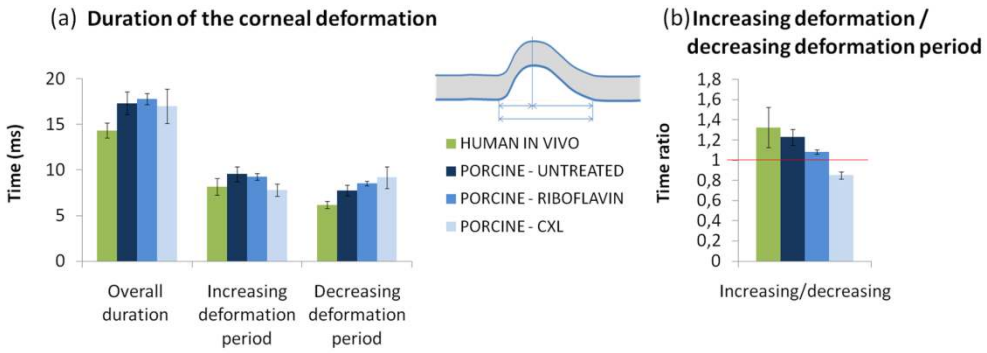

Fig. 6. (a) Duration of the corneal deformation parameters (overall deformation, increasing deformation period and decreasing deformation period) measured at the corneal apex, for the different conditions. (b) Time ratio (increasing deformation period/decreasing deformation period). The red horizontal line indicates the values at which the increasing deformation period duration equals the decreasing deformation period duration (time-symmetrical deformation).

temporal symmetry of the deformation. In untreated corneas (both human and porcine) the duration of the increasing deformation period was longer than the duration of the decreasing deformation period (corneal recovery), indicating that the peak deformation position was displaced toward the end of the overall deformation period (the effect being stronger for the human cornea). With treatments, the increasing deformation period (inward deformation) was reduced, while the decreasing deformation period (recovery time) obtained was longer. This effect is more clearly shown in Fig. 6b. The displacement of the peak symmetry toward the end of the ablation found in untreated corneas (increasing/decreasing time ratio > 1) was reduced with the treatments in porcine corneas. Deformation events after Riboflavin were almost temporally symmetrical. After UV-cross-linking, the temporal symmetry of the deformation was inverted, and the peak deformation displaced to the first half of the deformation period.

3.4. Deformation speed

Figure 7 shows parameters associated with the speed of the deformation at the corneal apex. The peak speed of the increasing deformation period (first period of the deformation event) was quite constant across conditions (see Fig. 7.a), around 0.12 mm/ms. However, the peak speed of the decreasing deformation period (peak deformation recovery speed) was different

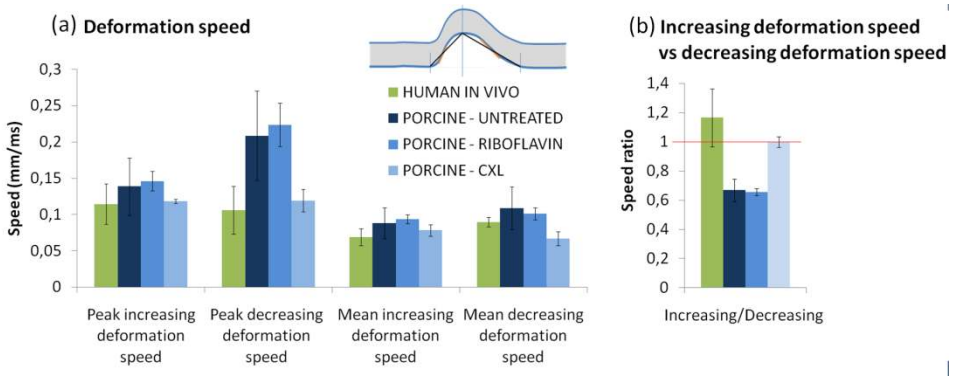

Fig. 7. (a) Deformation speed at the corneal apex, for the different conditions, obtained from measurements at the apex. (b) Peak-Speed ratio (increasing deformation period/decreasing deformation period). The red horizontal line indicates the values at which the peak deformation speed of the increasing deformation period equals the peak speed of the decreasing deformation period.

#159961 - $15.00 USD Received 13 Dec 2011; revised 17 Jan 2012; accepted 17 Jan 2012; published 9 Feb 2012

across conditions: 0.11 mm/ms for the human cornea, 0.21 for the untreated and Riboflavin porcine corneas, and 0.12 for the UV-cross-linked corneas, indicating a much slower deformation recovery after UV-cross-linking. The trends were similar for mean speeds (instead of peak speeds), although with reduced differences across conditions and lower values.

Figure 7b shows the ratio of the peak-deformation-speed in the increasing deformation period vs the decreasing deformation period (speed of recovery). In human corneas this ratio was close to unity. Both untreated and Riboflavin porcine corneas had ratios well below unity (0.66), indicating a peak deformation speed higher in the recovery than in the increasing (inward) deformation period. UV-cross-linked porcine corneas experienced an important increase in this ratio, which was found to be 0.999 ± 0.1, indicating an identical peak speed in both deformation periods.

3.5. Effects of treatment in the same eye

The previous comparisons between untreated and treated porcine eyes were based on the average values obtained for each condition. Figure 8 describes the longitudinal response of the same individual porcine eyes before and after the treatments. Data are represented in terms of ratios treated/untreated, with the treatment referring to Riboflavin + Dextran instillation and UV-cross-linking (left panel) or de-epitheliazation alone (right panel). The untreated reference condition corresponds to the measurements on the virgin eye. Figure 8 shows that all the parameters (except the overall duration of the deformation event) changed with the UV-cross-linking treatment, and that these changes were larger than the standard deviation across eyes.

The longitudinal results confirm the results of Figs. 5-7 on UV-cross-linking vs control group differences: (1) UV-cross-linking reduced the amplitude of corneal deformation; (2) Riboflavin + Dextran produced a decreased corneal thickness which was maintained after

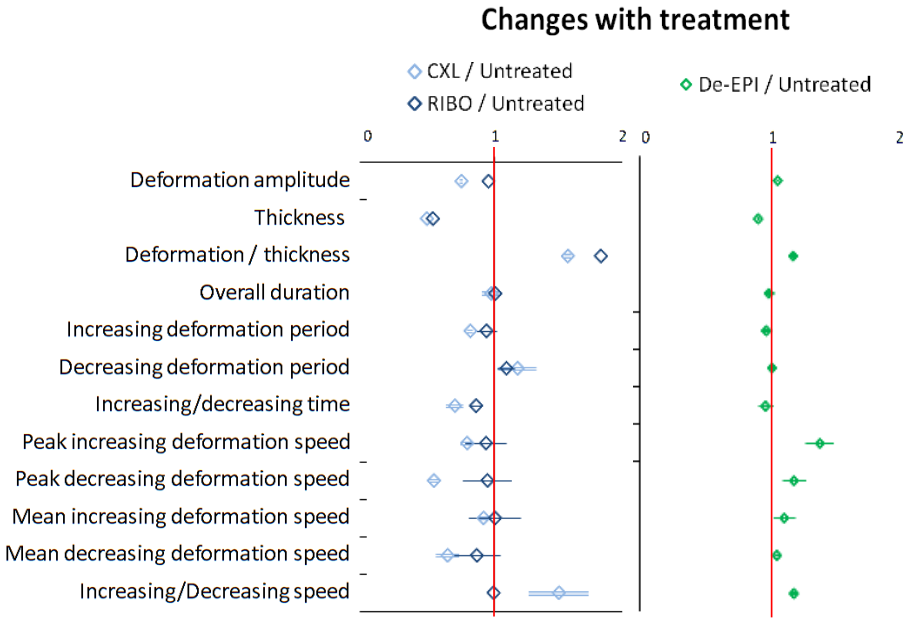

Fig. 8. Longitudinal changes induced in the parameters describing the dynamics of the corneal apex by different treatments on the same eyes. LEFT Panel: After de-epitheliazation and instillation of Riboflavin (RIBO, in neutral blue); and after additional UV-cross-linking (CXL, in light blue). Data of the left panel represent average and standard deviations of the evolution of different eyes. RIGHT Panel: After de-epitheliazation alone (De-EPI, in green). Data on the right panel represent average and standard deviation of repeated measurements of one eye.

#159961 - $15.00 USD Received 13 Dec 2011; revised 17 Jan 2012; accepted 17 Jan 2012; published 9 Feb 2012

UV-cross-linking; (3) deformation/thickness ratios changed with both treatments; (4) Treatments induced changes in the temporal displacement of the peak deformation; (5) UV-cross-linking decreased the deformation speed; (6) UV-cross-linking increased the speed ratio (increasing / decreasing deformation speed). In addition, the longitudinal analysis (Fig. 8) reveals additional findings for the Riboflavin condition, which were likely masked by individual variability of the eyes in the cross-sectional analysis: Riboflavin produced changes in temporal symmetry (like those already observed in UV-cross-linking condition in the cross-sectional analysis) and reduced the deformation mean and peak speeds (except for the mean speed in the increasing deformation period).

While the treatments with Riboflavin and, more importantly, UV-cross-linking are expected to change the biomechanical properties of the tissue, there are other structural changes likely changing the dynamic response of the cornea to the air puff event. The right panel of Fig. 8, representing the results for de-epitheliazation alone, is shown as a reference. De-epitheliazation reduces corneal thickness, therefore inducing some changes in the corneal response to the air puff, but it is not expected to affect the biomechanical properties of the tissue. Figure 8 (right panel) shows these measured changes. All the parameters, except those related to temporal durations and mean speeds, were statistically significant (unpaired t-tests, $p<0.05$). The deformation amplitude was slightly increased and therefore the deformation/amplitude ratio, and the deformation speeds were also increased, although mean speed changes were not significant. The increasing/decreasing speed ratio was also increased by de-epitheliazation alone.

3.6. Imaging the deformation of the full cornea

Figure 9 describes the deformation parameters (see Fig. 2b for a schematic diagram of the same) obtained from dynamic images of horizontal cross-sections of the cornea (as those shown in Fig. 4) in porcine eyes with different treatments. The deformation diameter (5.7 ± 0.8 mm in the untreated corneas) was reduced with the treatments (5.1 ± 0.3 mm after Rivoflavin and 4.4 ± 0.1 after UV-cross-linking). The reduction in deformation diameter after UV-cross-linking was statistically significantly different ($p<0.02$; two-sample t-test with unequal variances): 23% with respect to the untreated condition, and 14% with respect to the Riboflavin condition.

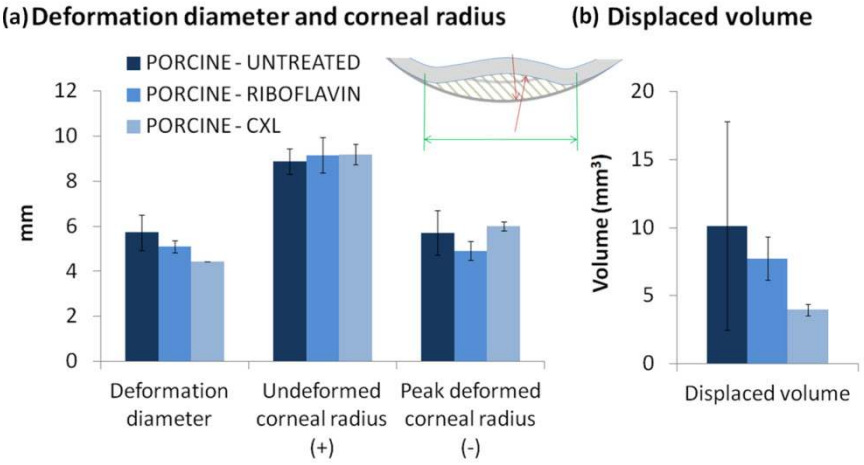

Fig. 9. Deformation parameters from dynamic images of the spatial deformation of the cornea (B-scan measurements along the horizontal meridian), for porcine in vitro eyes with different treatments. (a) Deformation diameter, non-deformed corneal radius and peak deformed corneal radius (the curvature sign is inverted in all cases). (b) Displaced volume. Error bars indicate the standard deviations across measurements on different eyes.

#159961 - $15.00 USD Received 13 Dec 2011; revised 17 Jan 2012; accepted 17 Jan 2012; published 9 Feb 2012

The radius of the stable non-deformed porcine corneas (8.9 mm) did not significantly change across treatments. However, the deformed corneal radius (measured at the moment of peak deformation) was reduced with Rivoflavin (from 5.7 to 4.9 mm), but it was later significantly increased (6.0 mm; $p<0.02$) by UV-cross-linking. The sign of the fitted radius was reversed in all the deformed corneas, indicating an inversion of the curvature of the cornea, as already shown in Fig. 4.

Figure 9b shows the corneal volume displaced by the air puff, at the moment of maximum deformation. UV-cross-linking produced a large decrease of displaced volume, from 10.1 mm^3 in untreated corneas and 7.7 mm^3 in corneas with Riboflavin, to 4.0 mm^3 (on average across eyes). The high variability found in untreated corneas (in accordance with the high variability observed in the deformation amplitude, see Fig. 5a) was reduced with Riboflavin + Dextran instillation.

Although the cornea moves at high speed during the deformation event (Fig. 7), the exposure time for each A-scan is only 15 us, preventing motion-blur. However, due to the sequential acquisition, some corneal points appear retarded with respect to others in the horizontal cross-sectional images. For peak corneal deformation speed the delay of some points with respect to other laterally displaced points (and therefore scanned at a different time) induces the observed slight asymmetries in the images of the full deformation (see Media 1), which are therefore likely to arise from scanning. However, the quantitative measurements provided in Fig. 9 refer to the time point of maximum deformation amplitude, in which the deformation speed is zero, for which this effect is not present. In fact, around the peak deformation time, the cornea appears stable (with several consecutive frames superimposed) and with maximum symmetry.

4. Discussion

We have demonstrated a new technique for the non-invasive imaging of the dynamic response of the cornea to an air puff inducing deformation, based on high-speed sOCT. The non-collinear configuration has allowed both for the high-speed evaluation of the dynamics of the corneal apex [39], and the imaging of the spatial corneal deformation over corneal cross-sections [30,31].

This new generation of imaging techniques in-vivo will potentially provide biomechanical information in individual eyes, avoiding the limitations of prior in-vivo techniques [23–25,42] (which provided only indirect information) and of in vitro techniques such as extensiometry [15] (which alter the anatomical integrity of the eye) or corneal button/whole eye inflation models [16,21] (which are subject to hydration and preservation issues).

The sensitivity of the technique has proven to be higher than existing techniques, as differences in corneal deformation dynamics across species and treatments are clearly detected. Furthermore, the entire deformation process can be dynamically visualized and studied quantitatively, allowing direct extraction of deformation parameters.

For untreated porcine eyes, the different hydration states are the main source of variability across eyes. In treated porcine eyes, dehydration reduces this effect, and individual differences across eyes in tissue properties appear. In human eyes, the reduced signal to noise ratio introduces some uncertainty in the image analysis, but it is very low compared with the variability introduced by eye movements and positioning errors (not present in in vitro eyes).

Despite the lower thickness of the human cornea as compared to the porcine corneas, the lower deformation amplitude (as well as shorter deformation durations and reduced deformation speeds) found in the study is indicative of a higher stiffness of human corneal tissue, in agreement with previous comparative reports of human and porcine corneal biomechanical properties [6,17]. However, this result could be affected by differences in the geometry and intraocular pressure across the tested eyes.

In porcine corneas in vitro, where intraocular pressure was kept constant across eyes and treatments, we found a significantly different corneal response across conditions: virgin

#159961 - $15.00 USD Received 13 Dec 2011; revised 17 Jan 2012; accepted 17 Jan 2012; published 9 Feb 2012

corneas, corneas after de-epitheliazation, after instillation of Riboflavin, and after UV-induced cross-linking. The corneal response after the UV-cross-linking treatment (and, to a minor extent, after Riboflavin) is consistent with an increase in corneal stiffness, as it produces reduced deformation amplitudes, reduced displaced volumes, and reduced deformation speeds to the same air-puff stimulus. This result is consistent with other studies aiming at estimating biomechanical properties of the cornea, following different approaches and time scales [5,21]. This study also shows that Riboflavin and UV-cross-linking produce changes in the temporal symmetry of the deformation event (a displacement in the peak amplitude toward the start of the deformation). The corneal recovery period is longer, and is also slower, compared to virgin and de-epithelialized corneas. The increasing/decreasing speed ratio appears as a very sensitive parameter to differences in treatment: it is increased with de-epitheliazation, reduced to the virgin corneas values after Riboflavin instillation (although with slightly reduced absolute speeds), and strongly increased with UV-cross-linking (with the absolute speeds reduced much more), indicating that the speed reduction is more important in the recovery period. These temporal and speed changes between the periods of increasing deformation and recovery suggest marked changes in the viscoelasticity of the tissue.

The different corneal responses (to the same deformation stimuli) obtained after treatments indicate that there are marked biomechanical changes induced on the cornea. These differences are revealed by geometrical changes at a macroscopic scale upon deformation, but are likely the result of changes in the microscopic structure of the cornea. The relative contribution of the corneal geometry (mainly changes in thickness, and to a lesser extent in curvature), intraocular pressure and material constituent properties to the effect remains an interesting question, where the experimental data can provide insights.

De-epitheliazation alone (right panel of Fig. 8), which only produces a small reduction in corneal thickness (10%) and minimal changes in the stromal arrangement, produces some changes in speed deformation parameters (but not other parameters), indicating a minor contribution of the epithelium to corneal biomechanics. The fact that Riboflavin alone produces significant changes in corneal deformation (in comparison with virgin corneas) is highly consistent with recent reports both from inflation models [23] and non-linear microscopy observations of collagen packing in Riboflavin + Dextran treated corneas [41], indicating both geometrical and ultra-structural changes. The instillation of Riboflavin + Dextran, and the subsequent corneal dehydration, also results in a reduction of corneal thickness (by 48%, Fig. 5a and Fig. 8), which is maintained after UV-cross-linking. However, the deformation parameters are capable of discriminating significantly across treatments (Fig. 8): the deformation amplitude and the deformation speeds are decreased with Riboflavin and UV-cross-linking (while they are increased with de-epitheliazation alone) and the temporal distribution is affected (while it was not with de-epitheliazation). The difference in behavior is more apparent if we consider that all the treated corneas (with Riboflavin, followed by UV-cross-linking or not) have been previously de-epithelialized. The differences in the deformation patterns that change with corneal thickness, cannot explain the changes in the biomechanical response observed after Riboflavin and UV-cross-linking. Conversely, the small change observed in the amplitude of the corneal deformation after Riboflavin, which is very similar to that of virgin eyes (Fig. 5 and Fig. 8) despite the drastic decrease (almost 50%) in thickness, cannot be explained by a thickness change alone. The strong reduction in deformation amplitude (26%) between UV-cross-linking and Riboflavin treated corneas (with similar thickness), reveals the changes induced by UV-cross-linking at the microscopic level, and the stiffening effect of the UV-cross-linking treatment.

Our results also show that the deformation diameter and the displaced volume are reduced with the treatments, which also change the radius of the deformed cornea (Fig. 9). Corneal curvature (and differences across eyes and conditions) could play a role in corneal deformation. Although corneal steepening has been reported clinically during the first month following UV-cross-linking [43], and this was observed also 24-hours after treatment in an in

#159961 - $15.00 USD Received 13 Dec 2011; revised 17 Jan 2012; accepted 17 Jan 2012; published 9 Feb 2012

vitro model [21], differences in corneal radius of curvature were negligible immediately following treatment. This was further confirmed in our study, by imaging horizontal sections of the non-deformed corneas at constant pressure (Fig. 9).

We have demonstrated a technique for the evaluation (in vivo and in vitro) of dynamic corneal deformation, capable of detecting differences across species and treatments. Temporal (Figs. 6, 7 and 8) and spatial (Fig. 9) measurements provide complementary (or even coincident—Fig. 5) descriptions of the deformation event. In particular, using this technique, we have confirmed non-invasively that UV-cross-linking induces changes in the corneal biomechanical properties, as recently reported using invasive techniques [21,41]. The differences must be the result of changes in constituent properties of the cornea, and not solely the results in changes in corneal thickness, geometry or IOP, as these were constant across some of the conditions.

The retrieved deformation parameters (amplitude, radius, diameter and volume of the deformation, as well as duration and speeds of the deformation periods), in combination with measurements of corneal biometry and IOP, pulse calibration, will be extremely valuable experimental data in corneal biomechanical models. Although these findings are of interest in the understanding of tonometric measurements of the cornea, the ultimate goal is to obtain the biomechanical properties of the tissue based on image-based measurements of corneal deformation. This information will serve as experimental inputs in finite element models of the normal, pathological and treated cornea [23], at an individual level, to improve diagnosis and prognosis of the disease and treatment. The developed technology can also help to understand the sources of the variation in the deformation response across corneas and conditions, including biomechanical properties of the tissue (elasticity and viscoelasticity), the changes in the structural properties of the corneas (as geometry) or the effect of IOP pressure (which was kept constant in our experiment).

5. Conclusions

The combination of high-speed sOCT imaging with air puff deformation shows a great potential as a research and clinical tool to retrieve the biomechanical properties of individual corneas, in vivo.

The non-collinear configuration presented in this study, makes available both, images of the corneal deformation over full corneal cross-sections, and also high speed measurements of the temporal evolution of the corneal apex.

The quantitative description provided by the set of deformation parameters proposed has proven to be sufficiently sensitive to detect, not only differences across species and treatments, but also across individual eyes. The differences found must be the result of changes in constituent properties of the cornea, and not a consequence of changes in corneal thickness, geometry or IOP.

These measurements could serve as potential inputs to be used in finite element models of the normal, pathological and treated cornea, and are a first step for the estimation of the biomechanical properties of corneal tissue, at an individual level and in vivo, to improve diagnosis and prognosis of diseases and treatments.

Acknowledgments

We are grateful to Enrique Gambra for helpful suggestions at the initial stages of this research and to David Lobato (INDO Equipment Group, Alcobendas, Madrid, Spain) for technical support. This research was funded by Spanish Ministry of Science and Innovation Grants # FIS2008-02065, FIS2011-25637; EURHORCs-ESF EURYI Award 05-102-ES, and ERC-2011-AdG294099 to S. M.

#159961 - $15.00 USD Received 13 Dec 2011; revised 17 Jan 2012; accepted 17 Jan 2012; published 9 Feb 2012